Small Angle X-Ray Scattering (SAXS) on Droplet Size and Liquid Contents of Condensed Supercritical Ethylene Jets

K.-C. Lin*
Taitech, Inc.
Beavercreek, Ohio 45430

Michael Ryan
Universal Technology Corporation

Campbell Carter
Air Force Research Laboratory

Alec Sandy, Suresh Narayanan, Jan Ilavsky, Jin Wang
Argonne National Laboratory

Abstract

The structures of condensed supercritical ethylene jets injected into a quiescent sub-critical environment were explored, using the small-angle x-ray scattering (SAXS) technique. The experiment was conducted at the 8-ID beamline at the Argonne National Laboratory. Droplet size and liquid volume fraction within the injected ethylene plume were measured. Effects of injection temperature and injector internal geometries on droplet size and liquid content were investigated. It was found that the SAXS technique is capable of measuring droplet size and liquid contents inside a dense jet, which is opaque in conventional diagnostic techniques. The droplet size inside a condensed supercritical ethylene jet is on the order of 100 nm, which is much smaller than that generated from industrial atomizers. The droplet size population, which makes significant liquid volume contributions, is distributed within a specific narrow range for each condensed ethylene jet. The average droplet size weighted by liquid volume fraction increases with both axial and radial distance within the condensed jet, due to droplet evaporation and gas expansion processes. The injection temperature is the most dominant factor in determining droplet size and liquid contents inside a condensed ethylene jet. At an injection temperature close to the ethylene critical temperature, the injected plume contains bigger droplets and higher liquid contents. Based on the present measurements, the effects of injector internal configuration on droplet size and liquid contents cannot be clearly verified.

Introduction

Injection of supercritical fluid is an increasingly important research area in the development of supersonic combustion ramjet (scramjet) technologies [1]. The use of endothermic hydrocarbon fuels as primary coolant around airframe and combustor components inevitably creates thermally cracked hydrocarbon mixtures at supercritical conditions [2]. The subsequent injection of the supercritical fluid into the scramjet combustor, which is typically at subcritical conditions, can considerably affect the combustion behavior of an engine, due to liquid generation through homogeneous nucleation processes [3].

The global structures of supercritical jets injected into a quiescent environment have been explored by Wu et al. [4,5] and Lin et al. [3], using shadowgraph images and Raman scattering. The effects of injection conditions on global appearances of the jets were characterized and the distribution profiles of the injected species at the downstream location were explored in these studies. Figure 1 illustrates the shadowgraph images of supercritical ethylene jets injected at various injection temperatures. The global jet appearance changes from transparent at a high injection temperature (Figure 1(a)) to opaque at a temperature close to the critical temperature (Figure 1(c)).

For the jet in Figure 1(c), the expansion process brings the supercritical fluid into a two-phase thermodynamic region to initiate droplet nucleation and growth, generating high-density small droplets within the injected plume [3-5]. The study of Lin et al. [3] even shows that the nucleation process can readily occur inside the injector. When probed with visible light sources, the multiple scattering among the high-density droplets within the ethylene plume contributes to the opaque appearance of the jet in Figure 1(c).

*Corresponding author, Kuo-Cheng.Lin@wpafb.af.mil

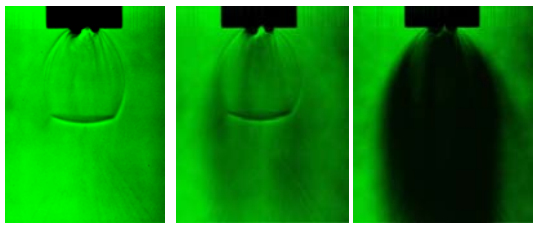

Figure 1. Shadowgraph images of supercritical ethylene jets injected from Injector #4 at various temperatures into a quiescence chamber filled with nitrogen at 137 kPa (20 psia). The Injection pressure is 5.15 MPa (750 psia).

Further understanding on the liquid condensation process during the injection of supercritical fluid, however, was limited by the capability of conventional diagnostic techniques. Consequently, the fundamental mechanisms associated with the homogeneous nucleation process has not yet been resolved to give detailed information on droplet size, droplet number density, and liquid volume fraction inside the plumes of supercritical jets. The other challenges in exploring the condensed supercritical jet lie in the highly dynamic features of jet expansion processes and droplet evaporation phenomenon. The presence of Mach disk and barrel shocks in the jet plume, as can be seen in Figure 1(a), and the eventual disappearance of all droplets at the downstream location highlight the need of an advanced diagnostic technique. This technique should be able to overcome the undesired multi-scattering within a dense two-phase jet and also provide instantaneous non-intrusive capability in measuring droplet size and liquid contents without changing both the thermodynamic and fluid dynamic features of the original jet.

Recently, the small angle x-ray scattering (SAXS) technique have been successfully applied to characterize the nucleation and crystal growth of a broad range of components, including zeolites, polymers, colloids, and composite materials [6-9]. It is therefore of great interest to assess the feasibility of applying the SAXS technique to the study of supercritical jets. The x-ray source at the 8-ID beamline at the Argonne National Laboratory was utilized for the first time to probe the structures of supercritical jets. The innovative diagnostic approach as well as some preliminary results corresponding to droplet size and liquid volume fraction inside highly-condensed supercritical ethylene jets will be presented in this paper.

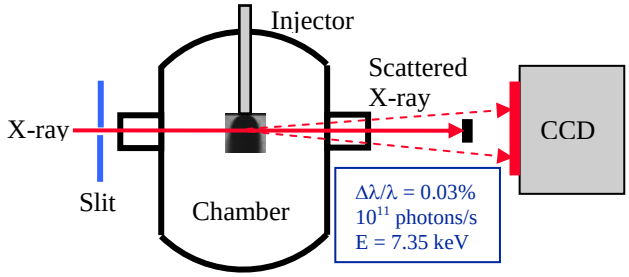

Figure 2. Schematic to illustrate the chamber setup and the optical layout of the present study

Experimental Methods

The experiment was conducted at the 8-ID beamline at the Argonne National Laboratory. Pure ethylene with desired temperature and pressure was injected into a chamber filled with nitrogen. The apparatus consists of an accumulator, a heating/chilling unit, a section of heat exchange tube, a solenoid valve, an injector, and the injection chamber. For the present study, the nitrogen pressure was set at 5.15 MPa (750 psia) for the accumulator. The critical pressure for ethylene is 5.04 MPa (733.54 psia). The test fluid was then introduced into the heat exchange tube to gradually reach the desired injection temperature. The injection temperature, which was measured immediately upstream the injection nozzle, was maintained between 283 K (T_r=1.00) and 306 K (T_r=1.08). The critical temperature for ethylene is 282.4 K.

Once the test fluid reached the desired temperature, a solenoid valve with a response time of 150 ms was opened for about 5-10 s to charge the test fluid into the injection chamber. Due to the transient behavior of the jet, data obtained during the first 2 seconds of injection was discarded. Before injection was begun, the injection chamber was flushed with nitrogen to remove oxygen and then filled with nitrogen. The initial pressure inside the injection chamber was selected at 137 kPa (20 psia). With the supply ethylene pressure of 5.15 MPa (750 psia), the initial

pressure ratio across the injection nozzle is 37.5. During the course of injection, a 20% to 40% increase in chamber pressure was observed by the end of injection. The chamber is equipped with two windows opposite to each other to provide x-ray access. Each window was equipped with a thin Kapton diaphragm, which has a high transmittance to x-rays. A simple schematic illustration of the experimental setup is shown in Figure 2.

Table 1. Geometries of the injection nozzles

Injector #	1	2	3	4	5
d (mm)	0.5	0.5	0.5	1.0	0.5
L/d	4	4	4	4	8
θ (°)	180	60	120	120	120

Five round nozzles with variations in orifice diameter (d), final passage length (L), and converging angle (θ) were used in the present study. The schematic in Figure 3 illustrates the internal geometries of the nozzle. Key parameters of each nozzle are tabulated in Table 1. Each nozzle begins with a 7.0-mm (0.276") diameter passage, followed by a converging section, which leads to the final passage. The final passage has a small converging angle of 2 degrees in order to ensure that the choke point can only occur at the nozzle exit, which has the desired orifice diameter (d). All transition corners are contoured surfaces to avoid any undesired flow separation. The entire internal surface of each nozzle was highly polished to ensure flow quality.

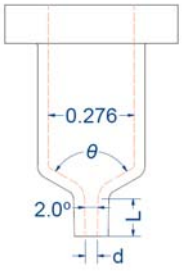

Figure 3. Internal injector geometries of the present study. Unit: inches.

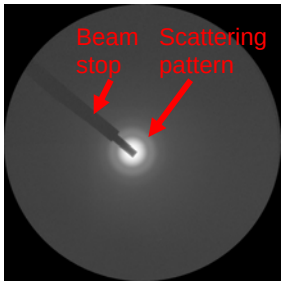

Figure 4. The typical small-angle scattering image for a highly-condensed supercritical ethylene jet. The beam stop was used to block the incoming x-ray.

A monochromatic, 0.1×0.1 mm^2 x-ray beam with a photon flux of ~10^{11} s^{-1} in the 8-ID beamline was directed through the supercritical ethylene plumes. Two different detectors were available for the present study: a CCD detector or a time-resolved photon-counting pixel array x-ray detector (PILATUS detector), resulting in slight variations in optical setup and detector operation. Figure 4 illustrates the typical scattering image from a CCD detector.

Creation of the radial scattering profile and particle size distributions from raw scattering images are accomplished in Igor Pro software using the Nika 1 and Irena macros, respectively, written by Jan Ilavsky [10,11]. Average volume fraction of condensed particles across the jet can be computed by integrating particle volume distribution. The accuracy of this quantity is dependent on the estimate for chord thickness where the beam crosses the jet as well as the estimate for scattering contrast between liquid ethylene and gaseous nitrogen/ethylene. Estimates for the chord thickness are dependent on an axisymmetric jet assumption and are taken from shadowgraph images of the jet at similar injection conditions.

In addition to scattering scans along the axis of the jet, it was desired to obtain some measure of the variation in condensation over the radius of the jet. An axisymmetric jet assumption made possible a simple tomographic analysis. Tomography was applied by scanning the x-ray beam from the center of the jet horizontally to the edge and decoupling the SAXS contribution at each radial bin for each scattering angle. A simple 3-pt Abel inversion was applied [12]. A slightly more accurate filtered back-projection (FBP) method [13] utilizing a generalized Hann window with a half value frequency of 0.8[14] was also applied to some data for comparison with the Abel inversion scheme. Both schemes returned negative inverted scattering for some conditions.

Results and Discussion

Droplet and Liquid Content Distributions

Figure 5 shows the droplet diameter vs. liquid volume fraction distribution profiles at various radial locations inside a condensed supercritical ethylene jet. The injection temperature of 284.8 K (53.2 F) creates a jet similar to the appearance of Figure 1(c). The Abel method was used to invert the SAXS contribution at each radial bin for each

scattering angle. The signal, however, was not scaled by the thickness of the scattering region, so the volume values are not exact in Figure 5. The measurement location is 1.0 mm from the nozzle exit.

First of all, the average droplet size weighted by volume, shown in Figure 5(b), decreases from 750 Å (75 nm) to 650 Å (65 nm) across the jet. These droplet sizes are very small compared to the typical droplet sizes generated from an industrial atomizer. Droplet populations up to 1000 Å (100 nm) were observed in Figure 5(a). These droplets, however, do not contribute to significant overall liquid volume due to their low number densities. According to the study of Lin et al. [15] based on the classic homogeneous nucleation theory, the estimated critical nucleus diameter is around 150 Å (15 nm) for an ethylene droplet at a supersaturation of 1.0 and a temperature of 270 K. Therefore, there is a substantial droplet growth from the nucleation incipient site, which is inside the injector [3], to the measurement location. Of course, droplet coalescence during droplet collision can also contribute to the increase in droplet size.

Second, the range of droplet size, which contributes to the significant portion of the condensed liquid volume, is relatively narrow for each measurement location in Figure 5(a). This observation indicates that the spatial region for most of the droplet nucleation to take place is also relatively narrow. This feature agrees with the typical homogeneous nucleation process. With the release of latent heat from nucleated droplets and the fast expansion process within the injector, the droplet nucleation rate appears reduced after reaching the peak value. This forms a narrowly-distributed droplet size population making a meaningful contribution to the condensed liquid volume.

Third, the total liquid volume fraction, calculated by integrating the distribution profiles over the diameter range, decreases with the radial distance from the jet axis, as can be seen in Figure 5(c). This trend indicates there is more liquid distributed at the central region of the jet. There is, however, no sufficient evidence to show whether the droplet nucleation or growth rate is actually higher at the central region inside the injector.

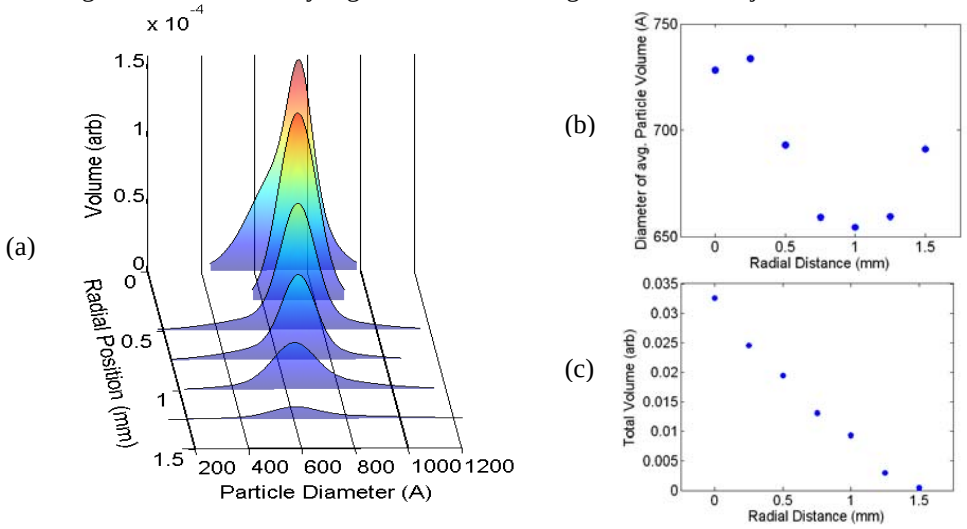

Figure 5. (a) Droplet diameter vs. liquid volume fraction distribution profiles, (b) Radial distribution of average particle size weighted by volume, (c) Radial distribution of the total liquid volume fraction. Injector #2, T_{inj}=284.8 K, x=1.0 mm.

Effects of Injector Geometry

The effects of injector geometry on the structures of supercritical ethylene jets are illustrated in Figure 6 and Figure 7, using Injector #1 and #2. The major difference between both injectors is the converging angle before the final passage. The injection condition was kept the same for both jets in Figure 6 and Figure 7. The presented data are treated with the FBP de-convolution scheme to obtain the radial distribution profiles of liquid volume fraction and volume-weighted droplet size at x=1.0 and 3.0 mm locations.

For the liquid volume fraction distribution at the x=1.0 mm location, Injector #2, which has a smaller converging angle, generates slightly more liquid at the core region (r=0 and 0.25 mm). The liquid volume fraction is almost the same at r≥0.5 mm for both jets. With more liquid at the core, the liquid containing region for the jet injected from Injector #2 at the x=3.0 mm location is slightly broader toward the jet center. Apparently, both jets exhibit a similar jet width from the same expansion ratio. The observed differences in liquid volume distribution must come from the differences in droplet nucleation and growth processes upstream the present axial probing location or even inside the injector. Efforts to explore the homogeneous nucleation process inside the injector should be carried out to address these observations.

The volume-weighted average droplet sizes range from 600 Å (60 nm) to 900 Å (90 nm) for Injector #1 in Figure 6 and from 600 Å (60 nm) to 800 Å (80 nm) for Injector #2 in Figure 7. At the x=3 mm location, larger droplets are mainly distributed at the peripheries of both jets, where heat transfer takes places and large droplets survive the evaporation process. There is no sufficient evidence to conclude whether the slightly larger droplets for the jet from Injector #1 at the x=3 mm location come from faster heat transfer (droplet evaporation) or upstream bigger droplets. Plume structures from other injectors in Table 1 exhibit similar distribution profiles. The effects of injector internal configuration on droplet size and liquid contents cannot be clearly verified in the present study.

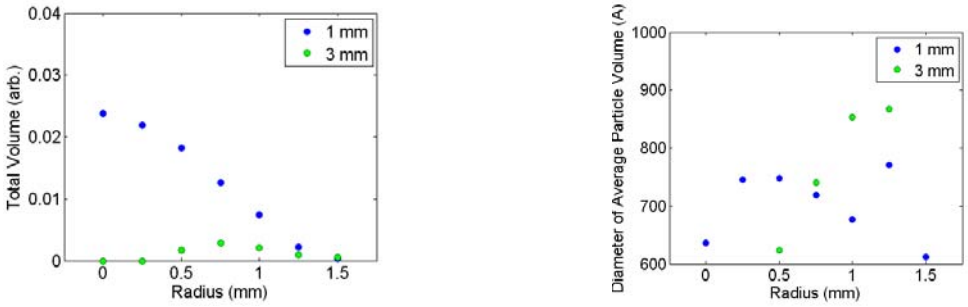

(a) (b)

Figure 6. Radial distributions of (a) Liquid volume fraction and (b) Volume-weighted droplet size for a supercritical ethylene jet at x=1.0 and 3.0 mm. Injector #1, T_{inj}=284.7 K. There are no droplet sizes for negligible liquid volume at r = 0 and 0.25 mm.

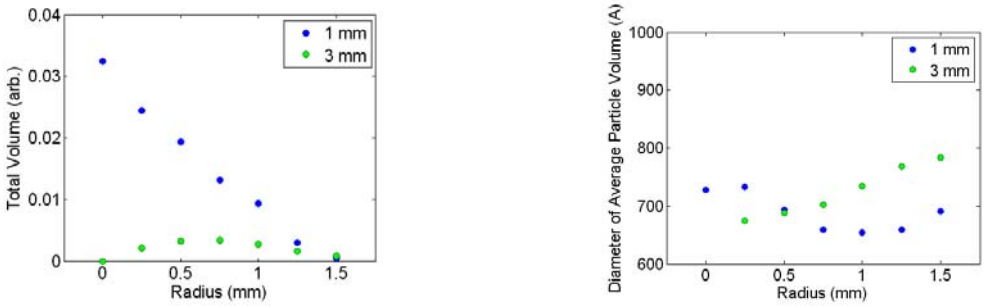

(a) (b)

Figure 7. Radial distributions of (a) Liquid volume fraction and (b) Volume-weighted droplet size for a supercritical ethylene jet at x=1.0 and 3.0 mm. Injector #2, T_{inj}=284.8 K.

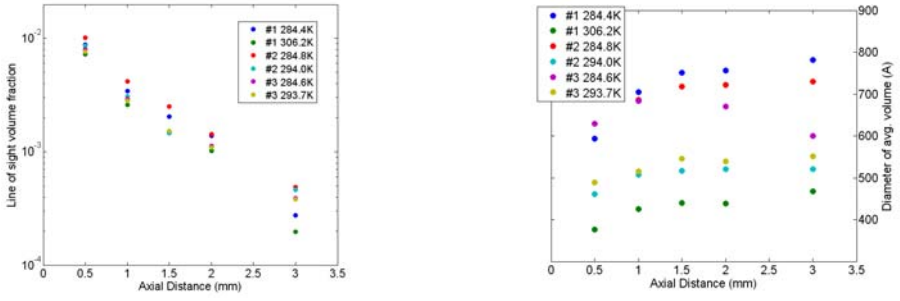

(a) (b)

Figure 8. Line-of-sight axial distribution of (a) liquid volume fraction and (b) volume-weighted droplet size for supercritical ethylene injected from various injectors at various temperatures. d_0=0.5 mm.

Droplet and Liquid Content Distributions

Figure 8(a) illustrates the axial line-of-sight distribution of the liquid volume fraction for supercritical ethylene injected from Injectors #1, #2, and #3 at various temperatures. Generally, the liquid volume fraction decreases exponentially with the axial distance for those test conditions in Figure 8(a). For the same injector, the injection condition with a high temperature generates less amount of liquid, as expected based on the observation in Figure 1. For the jets with the an injection temperature of 284 K, the general trends are Injector #2 generates the most liquid content

and Injector #3 produces the least liquid content in Figure 8(a). The effects of converging angle on the production of liquid phase can be easily drawn from this observation.

The corresponding axial distributions of volume-weighted droplet size are shown in Figure 8(b). Along the jet axis, the weighted droplet size is smaller than 800 Å (80 nm) for those conditions in Figure 8(b). The jets with an injection temperature close to the ethylene critical temperature produce larger droplets. The generated droplet size decreases as the injection temperature increases. Except for Injector #3 operated at a temperature of 284.6 K, the droplet size gradually increases with the axial distance. This is probably due to the faster rate of evaporation for small droplets. The sudden decrease in liquid volume fraction for Injector #3 at 284.6 K beyond 1 mm cannot be explained at this time. At the injection temperature of 284 K, Injector #1 produces larger droplets at $x \geq 1$ mm. Combined the observations in Figure 8, it is obvious that the jet with an injection temperature close to the ethylene critical temperature generates larger droplets and higher liquid content within the injected plume.

Conclusions

The structures of condensed supercritical ethylene jets injected into a quiescent sub-critical environment were explored, using the small-angle x-ray scattering (SAXS) technique. The experiment was conducted at the 8-ID beamline at the Argonne National Laboratory. Droplet size and liquid volume fraction within the injected ethylene plume were measured. Effects of injection temperature and injector internal geometries on droplet size and liquid content were investigated. It was found that the SAXS technique is capable of measuring droplet size and liquid content inside a dense jet, which is opaque in conventional diagnostic techniques. The droplet size inside a condensed supercritical ethylene jet is on the order of 100 nm, which is much smaller than that generated from industrial atomizers. The droplet size population, which makes significant liquid volume contributions, is distributed within a specific narrow range for each condensed ethylene jet. The average droplet size weighted by liquid volume fraction increases with axial distance and radial distance, within the condensed jet, due to droplet evaporation and gas expansion processes. Also, it was found that the injection temperature is the most dominant factor in determining droplet size and liquid contents inside a condensed ethylene jet. At an injection temperature close to the ethylene critical temperature, the injected plume contains bigger droplets and higher liquid contents. The effects of injector internal configuration on droplet size and liquid contents cannot be clearly verified in the present study.

Nomenclature

d	= injector orifice diameter	x	= axial position downstream of the injector exit centerline
L	= final passage length		
r	= droplet radius; also radial position in the jet	λ	= wave length
T_{inj}	= injection temperature	θ	= converging angle; also scattering angle
T_r	= reduced temperature		

Acknowledgements

Financial support from AFRL/Propulsion Directorate and facility support from Advance Photon Source at the Argonne National Laboratory are acknowledged.

References

1. Edwards, T., AIAA Paper 93-0807, Reno, NV, January, 1993.
2. Edwards, T. and Anderson, S. D., AIAA Paper 93-0806, Reno, NV, January, 1993.
3. Lin, K.-C., Cox-Stouffer, S., Kennedy, P., and Jackson, T., AIAA Paper 2003-0483, January 2003.
4. Wu, P.-K., Shahnam, M., Kirkendall, K. A., Carter, C. D., and Nejad, A. S., *Journal of Propulsion and Power* 15: 642-649 (1999).
5. Wu, P.-K., Chen, T. H, Nejad, A. S., and Carter, C. D., *Journal of Propulsion and Power* 12: 770-777 (1996).
6. Chattopadhyay, S., Erdemir, D., Evans, J., Ilavsky, J., Amenitsch, H., Segre, C., and Myerson, A., *Crystal Growth and Design* 5: 523-527 (2005).
7. de Moor, P., Beelen, T., and van Santen, R., *J. Phys. Chem. B* 103: 1639 (1999).
8. de Moor, P., Beelen, T., van Santen, R., Beck, L., and Davis, M., *J. Phys. Chem. B* 104: 7600 (2000).
9. Thiyagarajan, P., *J. Appl. Crystallogr* 36: 373 (2003).
10. http://www.uni.aps.anl.gov/~ilavsky/nika.html
11. http://www.uni.aps.anl.gov/~ilavsky/irena.html
12. Dasch, C.J., *Applied Optics* 31 (1992).
13. Kak, A.C. and Slaney, M., *Principles of Computerized Tomographic Imaging*, IEEE Press, New York, 2001.
14. Stearns, C.W., IEEE Nuclear Science Symposium Conference Record, 2005.
15. Lin, K.-C., Cox-Stouffer, S., and Jackson, T., *Combustion Science and Technology* 178: 126-160 (2006).